J. Fluid Mech. (1993), *vol.* 251, *pp.* 219–238

Isotropy of the small scales of turbulence at low Reynolds number

By J. KIM[1] AND R. A. ANTONIA[2]

[1] Center for Turbulence Research, NASA-Ames Research Center, Moffett Field, CA 94035, USA

[2] Department of Mechanical Engineering, University of Newcastle, New South Wales, 2308, Australia

(Received 4 November 1991 and in revised form 2 December 1992)

Spectral local isotropy tests are applied to direct numerical simulation data, mainly at the centreline of a fully developed turbulent channel flow. Despite the small Reynolds number of the simulation, the high-wavenumber behaviour of velocity and vorticity spectra is consistent with local isotropy. This consistency is verified by the relationship between streamwise wavenumber spectra and spanwise wavenumber spectra. The high-wavenumber behaviour of the pressure spectrum is also consistent with local isotropy and compares favourably with the calculation of Batchelor (1951), which assumes isotropy and joint normality of the velocity field at two points in space. The latter assumption is validated by the shape but not the magnitude of the quadruple correlation of the streamwise velocity fluctuation at small separations. There is only partial support for local spectral isotropy away from the centreline as the magnitude of the mean strain rate increases.

1. Introduction

Several tests can be applied for checking local isotropy in turbulent flows (e.g. Monin & Yaglom 1975). Antonia, Anselmet & Chambers (1986) underlined however that different tests may have different levels of sensitivity and therefore provide different measures of the departure from local isotropy. In particular, it was noted that mean square values of derivatives (of either velocity or temperature) weighted all of the spectrum so that deviations of these values from isotropy do not necessary indicate a breakdown in isotropy of the small scales of motion. Derivatives do show departures from local isotropy, when 'local' is interpreted to mean 'in physical space', as originally proposed by Kolmogorov (1941) and as used in most applications of the concept.

Indeed, the high-wavenumber regions of measured spectra of velocity fluctuations and of their derivatives appear to be consistent with local isotropy (e.g. Champagne 1981; Antonia *et al.* 1986; Antonia, Shah & Browne 1987). The wake data presented by Antonia, Shah & Browne (1987, 1988) were obtained for small turbulence Reynolds numbers ($R_{\lambda_1} = \overline{u_1^2}^{\frac{1}{2}} \lambda_1/\nu$, where u_1 is the longitudinal velocity fluctuation and $\lambda_1 = \overline{u_1^2}^{\frac{1}{2}}/\overline{u_{1,1}^2}^{\frac{1}{2}}$ is the longitudinal Taylor microscale, was in the range 40–80). At such Reynolds numbers, the spectral separation between the energy-containing part of the spectrum and the dissipation part of the spectrum is insufficient for an inertial subrange to exist. Nonetheless, the high-wavenumber regions of the velocity derivative spectra seemed to satisfy the isotropic spectral relations, allowing for the experimental uncertainty. The result implies that spectral local isotropy can be attained, independently of the Reynolds number. This implication is of some importance and, in the present paper, is tested against numerical data.

Direct numerical simulations (DNS) of turbulent flows (Kim, Moin & Moser 1987; Spalart 1988) have provided data that can permit a useful check of spectral isotropy, albeit at small Reynolds numbers. In this context, the simulations offer several advantages over hot-wire measurements. The use of Taylor's hypothesis – which is required in experiments for converting time derivatives to x_1 derivatives and for transforming the frequency n into a one-dimensional wavenumber k_1 ($\equiv 2\pi n/\bar{U}$, where $\bar{U}$ is the local mean velocity) – is avoided in the simulations. The general difficulties (e.g. Mestayer & Chambaud 1979) in inferring velocity derivatives from hot-wire signals at two points in space are absent in the simulations. Also, the x_2 resolution, especially in the wall region, is better for the simulations than for hot-wire measurements.

In a previous paper (Antonia, Kim & Browne 1991), the DNS data in a turbulent channel flow were used to examine the behaviour of the mean squared values of the velocity derivatives across the channel. It was concluded that the assumption of axisymmetry (or invariance of the derivative statistics with respect to rotation about a particular axis) generally provided a better approximation to these values than local isotropy. However, as noted above, mean squared values of velocity derivatives provide a different test for local isotropy from the behaviour of the high-wavenumber part of the derivative spectra. In view of the simplicity and theoretical importance of the concept of local isotropy, the present paper uses the same DNS data to examine in some detail the extent to which spectral local isotropy is satisfied. 'Spectral local isotropy' is used here – as in Van Atta (1977) – to signify the degree to which spectra of various quantities satisfy the appropriate isotropic relations when the wavenumber is sufficiently large. The particular quantities considered include the three velocity fluctuations, three vorticity fluctuations and the pressure fluctuation. To our knowledge, no previous attempt has been made to compare the high-wavenumber region of the pressure spectrum with the isotropic calculation of Batchelor (1951) or Heisenberg (1948) although several two-point pressure correlation calculations have been reported for isotropic turbulence (Batchelor 1951; Uberoi 1953; Hunt, Buell & Wray 1987) and measurements and calculations of the pressure spectrum have been made by Jones *et al.* (1979) and George, Beuther & Arnott (1984) up to wavenumbers extending slightly beyond the inertial subrange. Fung *et al.*'s (1992) recent calculation of the pressure spectrum using a kinematic simulation of homogeneous isotropic turbulence reproduced the $-\frac{7}{3}$ inertial range behaviour, in agreement with the results of George *et al.* (1984). Unlike experimental data, the DNS data provide spectral data in terms of wavenumbers in both the streamwise and spanwise directions. The comparison between streamwise wavenumber spectra and spanwise wavenumber spectra provides a further check of spectral isotropy.

A brief description of the database used in this study is given in §2. The isotropic form of various spectra is presented in §3, and this relationship is examined in §4 by comparing with the computed results. Further local isotropy tests using one-dimensional spectra and two-point correlations are given in §§5 and 6. The effect of Reynolds number on the high-wavenumber part of the spectra is considered in §7.

2. DNS database

The present study uses a database obtained from a direct numerical simulation of a fully developed turbulent channel flow at $Re = U_c h/\nu = 7900$, where Re is a Reynolds number based on the centreline velocity (U_c) and the channel half-width (h). This Reynolds number corresponds to $h^+ = hU_\tau/\nu = 395$ or $Re_\theta = U_c\theta/\nu = 700$, where

$U_\tau = (\tau_w/\rho)^{\frac{1}{2}}$, θ, and ν denote the friction velocity, the momentum thickness, and the kinematic viscosity, respectively. At the centreline, R_{λ_1} is equal to 53. In the computation, $256 \times 193 \times 192$ spectral modes – in the streamwise (x_1), normal to the wall (x_2), and spanwise (x_3) directions, respectively – were used. The spacings between collocation points were $\Delta x_1^+ \approx 7$, $\Delta x_2^+ \approx 0.05$ (near the wall) to 5.5 (at the centreline), and $\Delta x_3^+ \approx 4$, where the superscript + denotes the normalization by the friction velocity and the kinematic viscosity.

Turbulence statistics associated with this simulation are given in Kim (1989) and Antonia *et al.* (1991, 1992), and the reader may refer to these papers for the numerical algorithm and other details associated with the computation. With the spectral method used in the computation, the velocity field is advanced in the wavenumber space, and one-dimensional spectra are computed by summing over the other wavenumbers and time (in our case over several fields).

3. Isotropic spectra of velocity, vorticity and pressure fluctuations

For isotropic turbulence, the one-dimensional spectra of the three velocity components are well known and given in several texts (e.g. Batchelor 1953; Hinze 1959; Panchev 1971). The isotropic forms of the u_1, u_2 and u_3 spectra are written as

$$\phi_{u_1}(k_1) = \frac{1}{2}\int_{k_1}^{\infty} \frac{E(k)}{k}\left(1-\frac{k_1^2}{k^2}\right)\mathrm{d}k, \tag{1}$$

$$\phi_{u_2}(k_1) = \phi_{u_3}(k_1) = \frac{1}{4}\int_{k_1}^{\infty} \frac{E(k)}{k}\left(1+\frac{k_1^2}{k^2}\right)\mathrm{d}k, \tag{2}$$

where $\phi_{u_i}(k_1)$ $(i = 1, 2, 3)$ is the spectral density function of u_i, as a function of the one-dimensional wavenumber k_1 (in the x_1 direction). $E(k)$ is the three-dimensional spectrum which depends on the magnitude k of the wavenumber vector $\boldsymbol{k}$. The integrals $\int_{-\infty}^{\infty} \phi_{u_i}(k_1)\,\mathrm{d}k_1$ and $\int_0^{\infty} E(k)\,\mathrm{d}k$ equal the velocity variance $\overline{u_i^2}$ (no summation on i) and the kinetic energy per unit mass $\frac{1}{2}(\overline{u_1^2}+\overline{u_2^2}+\overline{u_3^2})$ respectively.

The isotropic relations for spectra of the velocity derivatives $u_{i,j}$ $(i = 1, 2, 3$ and $j = 1, 2, 3)$ were derived by Antonia *et al.* (1987). The spectrum of $u_{i,1}$ is given by

$$\phi_{u_{i,1}} = k_1^2 \phi_{u_i} \quad (i = 1, 2, 3). \tag{3}$$

The spectra of $u_{i,2}$ and $u_{i,3}$ are given by

$$\phi_{u_{1,2}}(k_1) = \phi_{u_{1,3}}(k_1) = \int_{k_1}^{\infty} \frac{E(k)}{4}\left(1-\frac{k_1^2}{k^2}\right)^2 k\,\mathrm{d}k, \tag{4}$$

$$\phi_{u_{2,2}}(k_1) = \phi_{u_{3,3}}(k_1) = \int_{k_1}^{\infty} \frac{E(k)}{4}\frac{k_1^2}{k}\left(1-\frac{k_1^2}{k^2}\right)\mathrm{d}k + \int_{k_1}^{\infty} \frac{E(k)}{16}\left(1-\frac{k_1^2}{k^2}\right)^2 k\,\mathrm{d}k, \tag{5}$$

$$\phi_{u_{2,3}}(k_1) = \phi_{u_{3,2}}(k_1) = \int_{k_1}^{\infty} \frac{E(k)}{4}\left(1-\frac{k_1^2}{k^2}\right)k\,\mathrm{d}k - \int_{k_1}^{\infty} \frac{E(k)}{16}\left(1-\frac{k_1^2}{k^2}\right)^2 k\,\mathrm{d}k, \tag{6}$$

with

$$\int_{-\infty}^{\infty} \phi_{u_{i,j}}(k_1)\,\mathrm{d}k_1 = \overline{u_{i,j}^2}.$$

Isotropic forms of the spectra of the vorticity fluctuation ω_i ($\equiv \epsilon_{ijk} u_{k,j}$, ϵ_{ijk} is the alternating tensor) were presented in Antonia *et al.* (1988), namely

$$\phi_{\omega_1}(k_1) = \frac{1}{2}\int_{k_1}^{\infty} \frac{E(k)}{k}(k^2 - k_1^2)\,\mathrm{d}k, \tag{7}$$

$$\phi_{\omega_2}(k_1) = \phi_{\omega_3}(k_1) = \tfrac{1}{2}k_1^2 \int_{k_1}^{\infty} \frac{E(k)}{k}\,\mathrm{d}k + \frac{1}{4}\int_{k_1}^{\infty} \frac{E(k)}{k}(k^2 - k_1^2)\,\mathrm{d}k, \tag{8}$$

with $$\int_{-\infty}^{\infty} \phi_{\omega_i}(k)\,\mathrm{d}k_1 = \overline{\omega_i^2}.$$

Since $E(k)$ is related to ϕ_{u_1} via (1), expressions for $\phi_{u_{i,2}}$ and $\phi_{u_{i,3}}$ can also be written in terms of $\phi_{u_{1,1}}$ (e.g. Van Atta 1991); similarly ϕ_{ω_2} and ϕ_{ω_3} can be expressed in terms of ϕ_{ω_1}.

The isotropic form of the pressure spectrum was derived by Batchelor (1951, 1953). Apart from assuming isotropy, the derivation also assumes Millionshtchikov's hypothesis (see Batchelor 1951, 1953) relating fourth-order and second-order two-point product mean values. The relation for the three-dimensional pressure spectrum $\Pi(k)$ follows from (8.3.18) and (8.3.19) in Batchelor (1953):

$$\Pi(k) = E(k)\int_0^{\infty} E(k')\, I\left(\frac{k}{k'}\right)\mathrm{d}k' \tag{9}$$

where I is a weighting factor given by

$$I(s) = \tfrac{1}{2}(s^2 + s^{-2}) - \tfrac{1}{3} - \tfrac{1}{4}(s + s^{-1})(s - s^{-1})^2 \ln\frac{1+s}{|1-s|}. \tag{10}$$

The one-dimensional pressure spectrum $\phi_p(k_1)$ is easily derived from $\Pi(k)$:

$$\phi_p(k_1) = \int_{k_1}^{\infty} \frac{\Pi(k)}{k}\,\mathrm{d}k \tag{11}$$

with $$\int_{-\infty}^{\infty} \phi_p(k_1)\,\mathrm{d}k_1 = \overline{p^2}.$$

Equation (11) is of course analogous to the relation between the one-dimensional temperature spectrum and the three-dimensional temperature spectrum (e.g. Hinze 1959, p. 285).

4. Verification of relations in §3

The determination of the integrals in the previous section require a knowledge of $E(k)$. As noted in Antonia *et al.* (1988), there are various ways of obtaining an expression for $E(k)$. In the approach adopted here, $E(k)$ is inferred from the energy spectrum $\phi_q(k_1)$, which is equal to the sum of the spectra of u_1, u_2 and u_3. The relationship between ϕ_q and $E(k)$ follows from (1) and (2):

$$\phi_q(k_1) = \phi_u(k_1) + \phi_v(k_1) + \phi_w(k_1) = \int_{k_1}^{\infty} \frac{E(k)}{k}\,\mathrm{d}k. \tag{12}$$

$E(k)$ is then given by $$E(k) = -k\left(\frac{\partial \phi_q}{\partial k_1}\right)_{k_1 = k}. \tag{13}$$

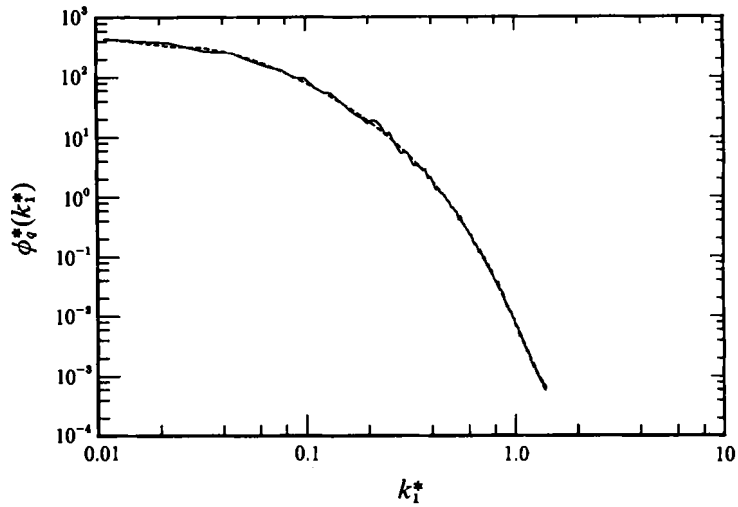

FIGURE 1. Turbulent energy spectrum at the centreline ($x_2/h = 1$): ——, ϕ_q^*; – – – –, least-squares (sixth-order polynomial) fit to ϕ_q^*.

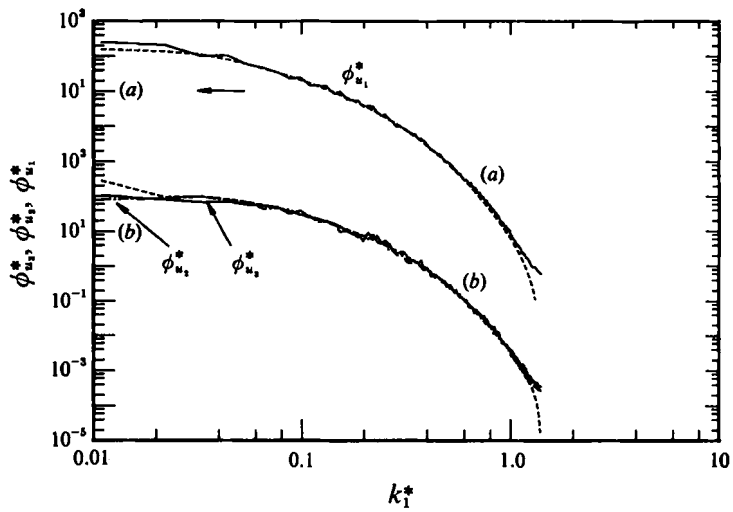

FIGURE 2. Comparison between u_1, u_2 and u_3 spectra ($x_2/h = 1$) and the isotropic calculations based on (1), (2) and (3). (Note the different origins for curves *a* and *b*.) (*a*) $\phi_{u_1}^*$, ——, *DNS*; – – –, calculation, equation (2). (*b*) $\phi_{u_2}^*$, – – – –, *DNS*; – – –, calculation, equation (2) $\phi_{u_3}^*$: ——, *DNS*; – – –, calculation, equation (2).

A high-order polynomial† fit of the form

$$\ln \phi_q^* = a_0 + a_1 x + \ldots + a_n x^n$$

was applied to the data. Note that $x = \ln k_1^*$ and the asterisk denotes normalization by the Kolmogorov scales $\eta \equiv (\nu^3/\bar{\epsilon})^{\frac{1}{4}}$ and $u_K \equiv (\nu\bar{\epsilon})^{\frac{1}{4}}$. (By definition, $u_K^+ \eta^+ \equiv 1$.) An adequate fit was obtained with $n = 6$ (figure 1). Starting with this fit, $E(k)$ was then obtained from (13) and subsequently used in the isotropic calculations of the velocity, vorticity and pressure spectra.

The comparison in figure 2, curve (*a*), between the u_1 spectrum and the isotropic relation, (1), indicates satisfactory agreement over the range $0.03 \lesssim k_1^* \lesssim 1$. In this

† The NAG subroutine used Chebychev polynomials (up to the 12th order) with a weighted least-squares criterion.

range, there is also good agreement (curve *b*) between ϕ_{u_2} or ϕ_{u_3} and the values obtained with (2). Note that the approximate equality between ϕ_{u_2} and ϕ_{u_3} is consistent with isotropy (and with the less stringent requirement of axisymmetry). The departure in curves (*a*) and (*b*) between the calculation and the data for $k_1^* \lesssim 0.03$ is not unexpected. The departure at the largest wavenumbers ($k_1^* > 1$) partly reflects small errors (as illustrated by the slight upturn) in the distributions of ϕ_{u_1}, ϕ_{u_2} and ϕ_{u_3} and also likely inaccuracies in $E(k)$. Distributions of ϕ_{u_2} (or ϕ_{u_3}) were also calculated using

$$\phi_{u_2} = \tfrac{1}{2}\phi_{u_1} - \tfrac{1}{2}k_1 \frac{\partial \phi_{u_1}}{\partial k_1} \tag{14}$$

and a polynomial fit to ϕ_{u_1}, similar to that used for ϕ_q. For $0.03 < k_1^* < 1$, the resulting calculation (not shown here) follows the DNS distributions of ϕ_{u_2} (or ϕ_{u_3}) as well as that in figure 2 (curve (*b*)). For $k_1^* > 1$, the agreement is better than in curve (*b*), due to the direct use of ϕ_{u_1} as input to the calculation.

Reasonable agreement can be observed in figure 3(*a*)(i) between the ω_1 spectrum and the calculation based on (7). There is somewhat better agreement, figure 3(*a*)(ii) and (iii), between the DNS distributions of ϕ_{ω_2} or ϕ_{ω_3} and the calculation based on (8). For clarity, the distributions of ϕ_{ω_2} and ϕ_{ω_3} are displaced in figure 3. These distributions are essentially identical, as can be inferred from the comparison with the calculated distribution, which is the same for ϕ_{ω_2} as for ϕ_{ω_3}. The near equality between ϕ_{ω_2} and ϕ_{ω_3}, like that between ϕ_{u_2} and ϕ_{u_3}, represents good support for axisymmetry. It should be noted that ϕ_{ω_2} and ϕ_{ω_3} can also be calculated by starting with ϕ_{u_1} instead of $E(k)$. Since

$$E(k) = k^2 \left(\frac{\partial^2 \phi_{u_1}}{\partial k_1^2}\right)_{k_1 = k} - k \left(\frac{\partial \phi_{u_1}}{\partial k_1}\right)_{k_1 = k}. \tag{15}$$

By substituting this expression in (7) and (8), it is easy to show that

$$\phi_{\omega_1}(k_1) = \phi_{u_{1,1}}(k_1) + 4 \int_{k_1}^{\infty} \frac{\phi_{u_{1,1}}}{k} \mathrm{d}k \tag{16}$$

and

$$\phi_{\omega_2}(k_1) \equiv \phi_{\omega_3}(k_1) = \tfrac{5}{2}\phi_{u_{1,1}}(k_1) - \frac{k_1}{2}\frac{\partial \phi_{u_{1,1}}}{\partial k_1} + 2 \int_{k_1}^{\infty} \frac{\phi_{u_{1,1}}}{k} \mathrm{d}k. \tag{17}$$

Equations (16) and (17) yield distributions, figure 3(*b*), which are in as good an agreement with the DNS distributions of ϕ_{ω_1} and ϕ_{ω_2} (or ϕ_{ω_3}) as the calculations shown in figure 3(*a*), up to $k_1^* \approx 1$. For larger wavenumbers, (16) and (17) are in better agreement with the DNS distributions since the DNS distribution of $\phi_{u_{1,1}}$ is used as input for the calculations based on (16) and (17).

The vorticity spectrum can be obtained from the sum of the spectra of the individual vorticity components, namely

$$\phi_\omega(k_1) = \phi_{\omega_1}(k_1) + \phi_{\omega_2}(k_1) + \phi_{\omega_3}(k_1). \tag{18}$$

The reasonable agreement between $\phi_\omega(k_1)$ and isotropy (i.e. (7) and (8) or (16), (17)), as shown in figure 3(*a*, *b*), follows from that between the individual components of ϕ_ω and the isotropic calculations. Note that $\phi_\omega(k_1)$ should represent the energy dissipation spectrum for homogeneous turbulence. Antonia *et al.* (1988) observed a close correspondence between approximations to the energy dissipation spectrum and the vorticity spectrum, measured in the self-preserving region of a cylinder wake. The

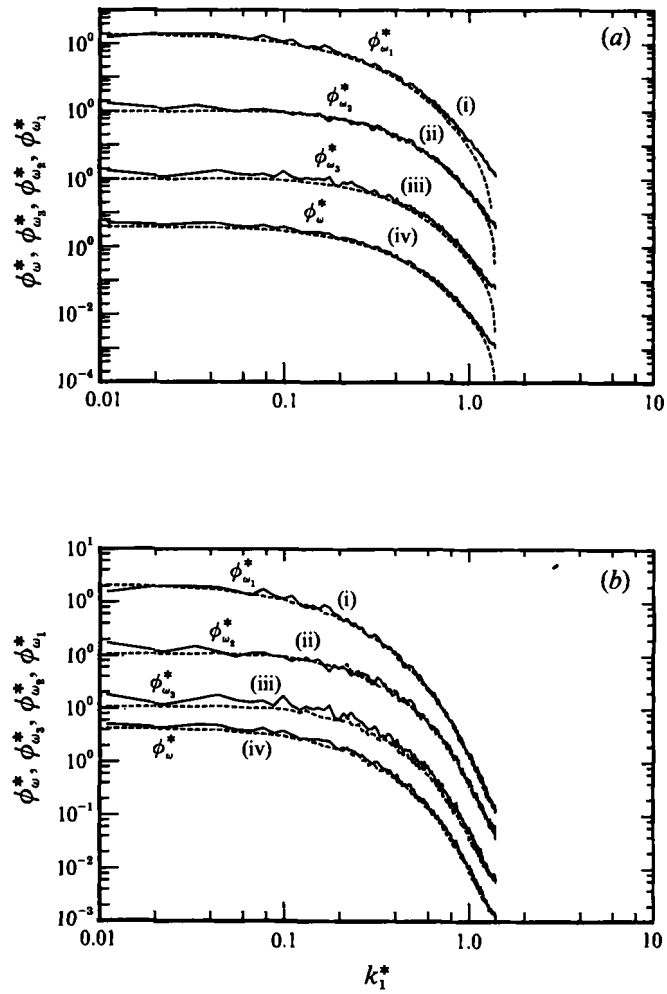

FIGURE 3. Comparison between ω_1, ω_2, ω_3 and ω spectra and isotropic calculations ($x_2/h = 1$). (Note the different origins for curves i, ii, iii and iv.) ——, DNS; — —, calculation. For (*a*) the calculations are based on (7), (8) and (13). For (*b*), the calculations are based on (16), (17) using the DNS distribution of $\phi_{u_{1,1}}$ as input.

present data closely satisfy the homogeneous relation $\bar{\epsilon} = \nu\overline{\omega^2}$ everywhere across the channel (Antonia *et al.* 1991) and the behaviour of $\phi_\omega(k_1)$ in figure 3 should therefore reflect closely that of $\phi_\epsilon(k_1)$.

The pressure spectrum ϕ_p^* is shown in figure 4 together with the isotropic calculation based on (9), (10) and (11). There is quite satisfactory agreement between the two distributions over more than a half decade in wavenumber extending up to nearly the Kolmogorov wavenumber ($k_1^* = 1$). For $k_1^* > 1$, the DNS distribution curls up a little (this may be a numerical effect but should not be of serious concern here as it is relatively small) while the calculation may become unreliable due to inaccuracies in fitting to $E(k)$ in this region. The agreement between the two distributions in figure 4 implies support for the two assumptions made in Batchelor's (1951) calculation. Further evidence for local isotropy of the pressure spectrum is given in §5 while the normality assumption is considered in §6. The agreement at relatively large k_1^* in figure 4 complements the agreement – primarily over the inertial subrange – between

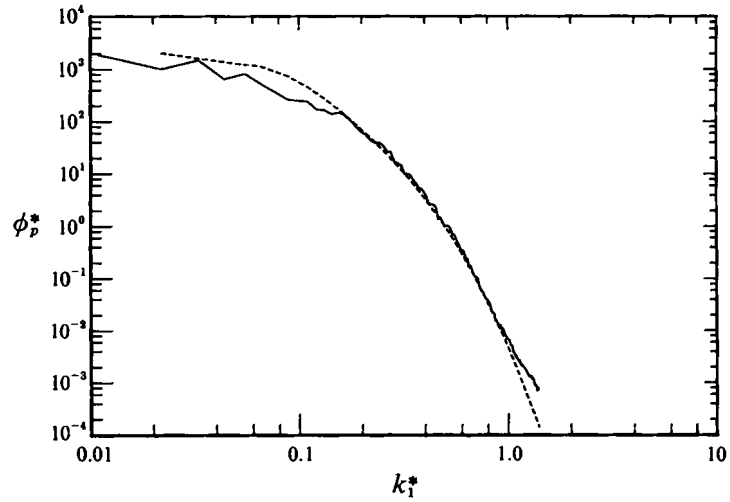

FIGURE 4. Comparison between the pressure spectrum ($x_2/h = 1$) and Batchelor's calculation. $\phi_p^*(k_1^*)$: ——, DNS; – – –, calculated using (9), (11) and (13).

measurement and isotropic calculation obtained by George *et al.* (1984) in the mixing layer of an axisymmetric jet.

5. Further checks of spectral isotropy and comparison with other flows

The relationship between computed spectra in the streamwise and spanwise directions provides a further test for isotropy.

Isotropic expressions for $\phi_{u_i}(k_3)$ can be derived by relabelling the indices in (2), i.e. $\phi_{u_1}(k_3) = \phi_{u_3}(k_1)$ or $\phi_{u_3}(k_1)$. Similarly one can show that $\phi_{u_2}(k_3) = \phi_{u_2}(k_1)$ or $\phi_{u_3}(k_1)$ while $\phi_{u_1}(k_1) = \phi_{u_3}(k_3)$. Figure 5(*a*) confirms that the 'longitudinal' spectra $\phi_{u_1}^*(k_1^*)$ and $\phi_{u_3}^*(k_3^*)$ follow each other closely except at low wavenumbers. Figure 5(*b*) contains the four 'lateral' spectra, namely $\phi_{u_2}^*(k_1^*)$, $\phi_{u_3}^*(k_1^*)$, $\phi_{u_1}^*(k_3^*)$ and $\phi_{u_2}^*(k_3^*)$. These spectra follow each other, at sufficiently large values of k_1^* or k_3^*, with approximately the same level of agreement as the 'longitudinal' spectra.

In the case of the scalar quantity p, one would expect that, for sufficiently large wavenumbers,

$$\phi_p(k_1) = \phi_p(k_3). \tag{19}$$

Figure 5(*c*) shows that $\phi_p^*(k_1^*)$ and $\phi_p^*(k_3^*)$ are in close agreement for k_1^* or $k_3^* \gtrsim 0.1$, thus providing good support for isotropy of the small-scale pressure fluctuations.

It is of interest to examine whether small-scale spectral isotropy can also be observed away from the centreline where the large-scale anisotropy is more pronounced than at the centreline. Deviations from isotropy are described in terms of anisotropy-invariant maps of dissipation and vorticity in Antonia *et al.* (1991). The relationship between k_1^* and k_3^* spectra at $x_2/h \approx 0.4$ ($x_2^+ = 160$) is shown in figure 6, the presentation being identical to that of figure 5. The mean strain rate at $x_2/h = 0.4$ is not negligible ($S\overline{q^2}/\bar{\varepsilon} \approx 6$, where S is the mean shear rate, and $\overline{q^2}$ is equal to twice the mean turbulent kinetic energy). The departure at low wavenumbers is slightly more pronounced in figure 6(*b*) than in figure 5(*b*). The degree with which the pressure spectrum satisfies high-wavenumber isotropy in figure 6(*c*) is similar to that in figure 5(*c*). At sufficiently large values of k_1^* and k_3^*, $\phi_{u_1}^*(k_1^*)$ and $\phi_{u_2}^*(k_3^*)$ follow each other (figure 6*a*) but they are not equal (the difference looks small because of the log–log coordinates), the k_1^*

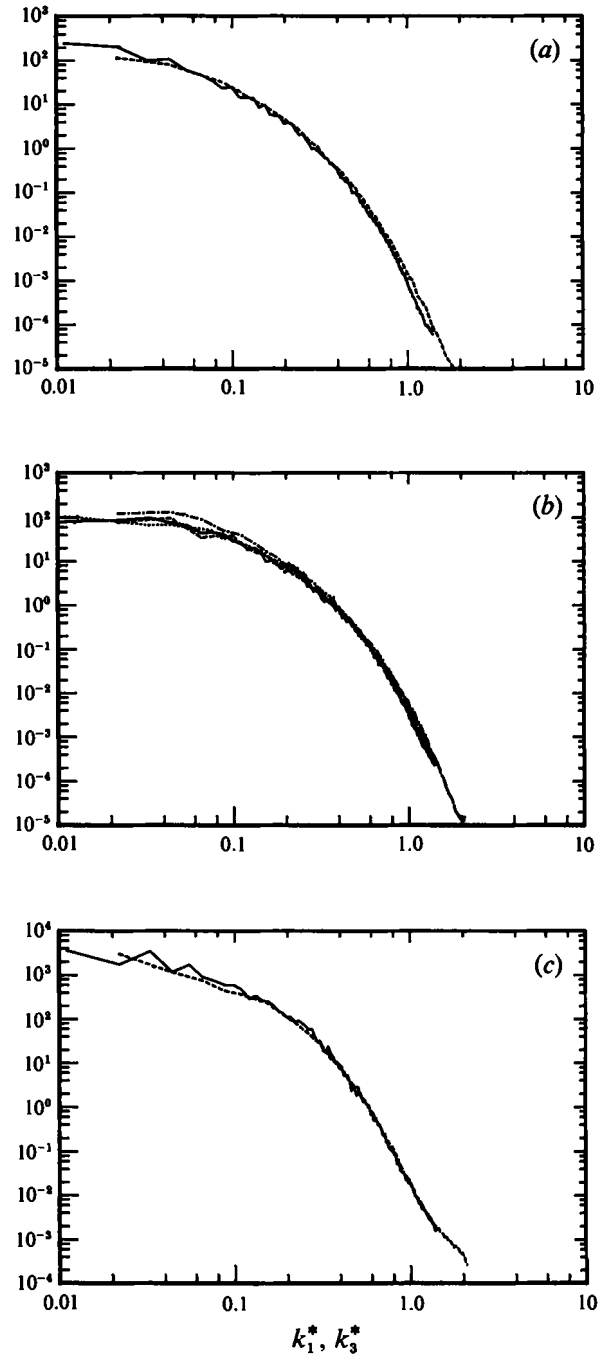

FIGURE 5. Comparison between velocity spectra in the streamwise and spanwise wavenumber spectra of velocity and pressure fluctuations at the centreline ($x_2/h = 1$). (*a*) ——, $\phi^*_{u_1}(k_1^*)$; – – – –, $\phi^*_{u_2}(k_3^*)$. (*b*) ——, $\phi^*_{u_2}(k_1^*)$; · · · · ·, $\phi^*_{u_2}(k_1^*)$; — — —, $\phi^*_{u_1}(k_3^*)$; – – – –, $\phi^*_{u_2}(k_3^*)$. (*c*) ——, $\phi^*_p(k_1^*)$; – – – –, $\phi^*_p(k_3^*)$.

spectrum falling below the k_3^* spectra. In figure 6(*b*), for sufficiently large wavenumbers, $\phi^*_{u_1}(k_3^*) \approx \phi^*_{u_2}(k_3^*)$ while $\phi^*_{u_2}(k_1^*) \approx \phi^*_{u_3}(k_1^*)$. These four magnitudes should however be the same (to satisfy local isotropy). As in figure 6(*a*), the k_1^* spectra lie below the k_3^* spectra. It is possible that these differences reflect a 'small' departure of the small scales

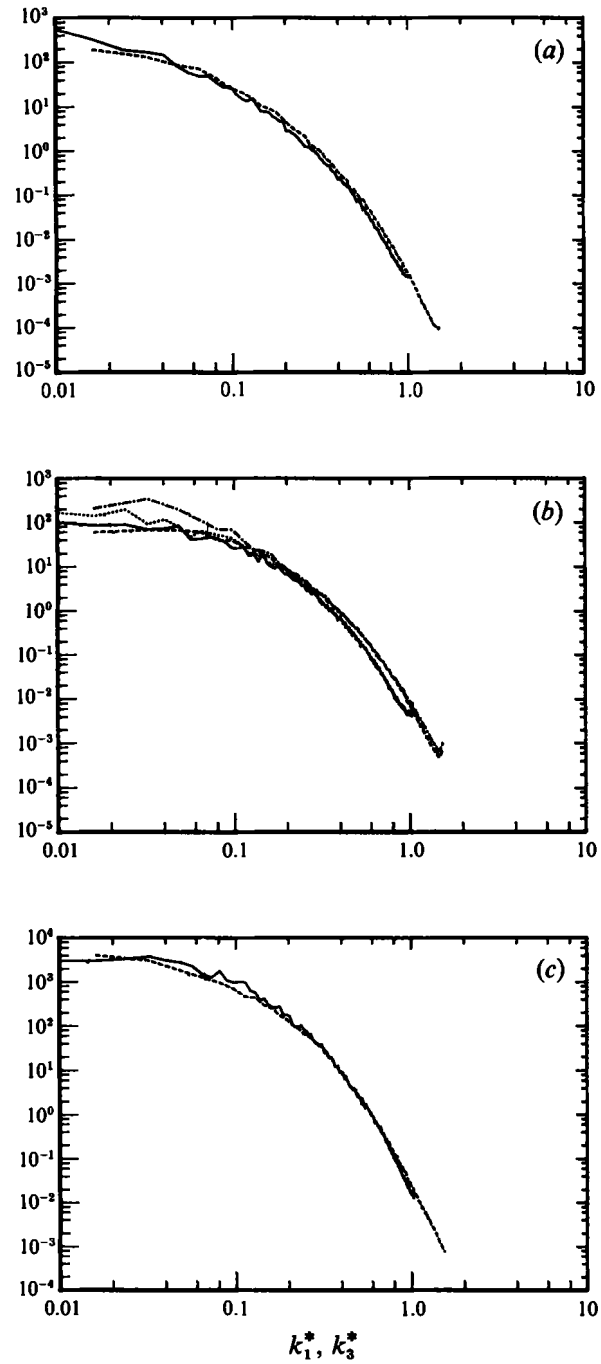

FIGURE 6. Comparison between streamwise and and spanwise wavenumber spectra of velocity and pressure fluctuations away from the centreline ($x_2/h \approx 0.4$). (*a*) ——, $\phi^*_{u_1}(k_1^*)$; – – – –, $\phi^*_{u_2}(k_3^*)$. (*b*) ——, $\phi^*_{u_2}(k_1^*)$; · · · · ·, $\phi^*_{u_3}(k_1^*)$; — — —, $\phi^*_{u_1}(k_3^*)$; – – – –, $\phi^*_{u_3}(k_3^*)$. (*c*) ——, $\phi^*_p(k_1^*)$; – – – –, $\phi^*_p(k_3^*)$.

from isotropy but a more reliable measure of this departure is needed (a possible measure is provided by the ratio shown in figure 7) before definite conclusions can be made. A more effective way of observing the departure is provided by the quantities plotted in figure 7 using linear scales. The quantities are the ratios of $\phi_{u_1}(k_3)$ or $\phi_{u_2}(k_3)$

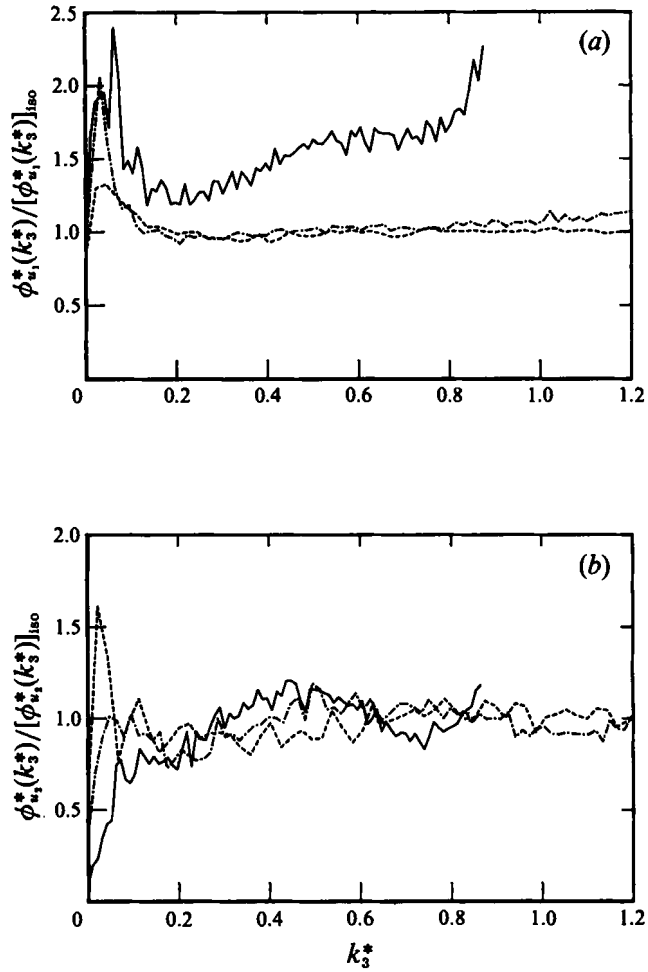

FIGURE 7. Ratio of $\phi^*_{u_1}(k_3^*)$ or $\phi^*_{u_2}(k_3^*)$ and its isotropic value, calculated from (2). (*a*) $\phi^*_{u_1}(k_3^*)/[\phi^*_{u_1}(k_3^*)]_{iso}$, (*b*) $\phi^*_{u_2}(k_3^*)/[\phi^*_{u_2}(k_3^*)]_{iso}$; ——, $x_2^+ = 40$; – – –, 160; – – – –, 395.

and the corresponding isotropic spectra. The distributions support previous conclusions inferred from the log–log plots. In particular, isotropy is closely satisfied for $\phi_{u_1}(k_3)$ and $k_3^* \gtrsim 0.2$ *at* $x_2^+ = 160$ and 395. There is more scatter in the case of $\phi_{u_2}(k_3)$ but the conclusion is unaltered. The departure from isotropy at low wavenumbers ($k_3^* \lesssim 0.2$) is indeed more emphasized in figure 7 than in figure 6.

The isotropy of small scales when $S\overline{q^2}/\bar{\epsilon}$ is sufficiently small and the possible departures from isotropy at larger values of $S\overline{q^2}/\bar{\epsilon}$ are not a peculiarity of this flow. Spalart's (1988) DNS boundary-layer distributions of $\phi^*_{u_1}(k_3^*)$, $\phi^*_{u_2}(k_3^*)$ and $\phi^*_{u_3}(k_3^*)$ at $y^+ = 200$ (figure 21*a* of this paper) show that $\phi^*_{u_1}(k_3^*)$ and $\phi^*_{u_2}(k_3^*)$ are in close agreement with isotropy (equation (2)) when $k_3^* \gtrsim 0.1$ (the maximum value of k_3^* was only 0.7). Results at $y^+ = 40$ (figure 21*b* of his paper) show that $\phi^*_{u_2}(k_3^*)$ was in reasonable agreement with (2) for $k_3^* \gtrsim 0.1$ but $\phi^*_{u_1}(k_3^*)$ was significantly underestimated by (2). The present spectra for $\phi^*_{u_1}(k_3^*)$ and $\phi^*_{u_2}(k_3^*)$ at $x_2^+ = 40$ ($S\overline{q^2}/\bar{\epsilon} = 7.6$) show very similar trends to those of Spalart. The degree to which $\phi^*_{u_2}(k_3^*)/[\phi^*_{u_2}(k_3^*)]_{iso}$ approximates 1 at $x_2^+ = 40$ is comparable to that at $x_2/h = 1$ ($x_2^+ = 395$). At $x_2^+ = 40$, the ratio $\phi^*_{u_1}(k_3^*)/[\phi^*_{u_1}(k_3^*)]_{iso}$ is however consistently greater than 1, the departure increasing as $k_3^* \to 1$.

There is somewhat mixed experimental support for small-scale isotropy, in the context of (1) and (2). For example, most of the distributions of $\phi_{u_2}(k_1)$ and $\phi_{u_3}(k_1)$ obtained by Comte-Bellot (1963) in a fully developed turbulent channel flow indicate varying degrees of departure from (2) when k_1 is sufficiently large† (these departures are certainly smaller than those at small k_1). The data show evidence of an increased departure from local isotropy as the wall is approached. There is however no evidence, at least when the strain rate is small, to support that the departure increases as the Reynolds number decreases. (For Comte-Bellot's data, h^+ is in the range 2300–8200, easily one order of magnitude larger than for the present simulations.) Klebanoff's (1955) measured v spectra in a turbulent boundary layer ($x_2/\delta = 0.05$ and 0.58) showed an asymptotic trend towards the isotropic calculation at large wavenumbers. Mestayer (1982) observed quite good agreement with (2) at $x_2/\delta = 0.33$ in a relatively high Reynolds number turbulent boundary layer. Champagne, Harris & Corrsin (1970) reported reasonable agreement between (2) and their measurements of $\phi_{u_2}(k_1)$ and $\phi_{u_3}(k_1)$ in a nearly homogeneous turbulent shear flow ($S\overline{q^2}/\bar{\epsilon} = 5.9$) when $0.04 \lesssim 0.5$. The deviation from (2) when $k_1^* > 0.5$ was attributed to spatial resolution limitations (both wire lengths and separation between the wires of the X-probe).

6. Pressure and velocity correlations at small separations

The correlation between the pressure fluctuations at two points is given by (Batchelor 1951, 1953)

$$P(r) = 2\overline{u_1^2}^2 \int_r^\infty \left(y - \frac{r^2}{y}\right)\left(\frac{\partial f}{\partial y}\right)^2 \mathrm{d}y, \tag{20}$$

where $P(r) = \overline{p(x)p(x+r)}$, $r = |r|$, f is the correlation coefficient $\overline{u_1(x)u_1(x+r)}/\overline{u_1^2}$. Relations similar to (20) were obtained by Oboukhov (1949) and Oboukhov & Yaglom (1951). As noted by Batchelor (1951), relation (20) is considerably simpler than (9), which relates $\Pi(k)$ to $E(k)$ ($\Pi(k)$ is obtained by Fourier transforming $P(r)$). Although (20) and (9) are equivalent, the advantage of (20) over (9) is that it circumvents the need to know the three-dimensional energy spectrum. Identifying r with r_1, the separation in the x_1 direction, the distribution of $f(r_1) = \overline{u_1(x_1)u_1(x_1+r_1)}/\overline{u_1^2}$ is shown in figure 8(*a*). Also shown is the distribution of the lateral correlation coefficient $g(r)$, calculated using the isotropic relation

$$g \equiv f + \frac{r_1}{2}\frac{\partial f}{\partial r_1}. \tag{21}$$

For small r_1, figure 8(*a*) shows that g is in quite reasonable agreement with the u_2 and u_3 correlation coefficients. It may be noted however that g is in slightly better agreement with the u_3 correlation than with the u_2 correlation. Correspondingly one should expect that at high wavenumbers, the spectral calculation (equation (2)) should be in slightly better agreement with ϕ_3 than ϕ_2. This is indeed the case although the difference between ϕ_2 and ϕ_3 is too small to be discerned on the log–log scale of figure 2(*b*).

Using the distribution of f shown in figure 8(*a*), $P(r_1)$ was calculated from (20). The calculated value of $P(0)$ was about 12% larger than the pressure variance indicated by the simulation (this increase is consistent with the larger magnitude of the calculated spectrum at low wavenumbers, figure 4). However, the shape of the calculated pressure correlation, expressed by the ratio $P(r_1)/P(0)$, is in very good agreement with the DNS data for r_1^* extending to about 20 (figure 8*b*). This agreement is of similar quality to

† Laufer's (1953) distribution of $\phi_2(k_1)$ on the centreline of a pipe showed a departure from (2) in the opposite direction to that of Comte-Bellot (1963).

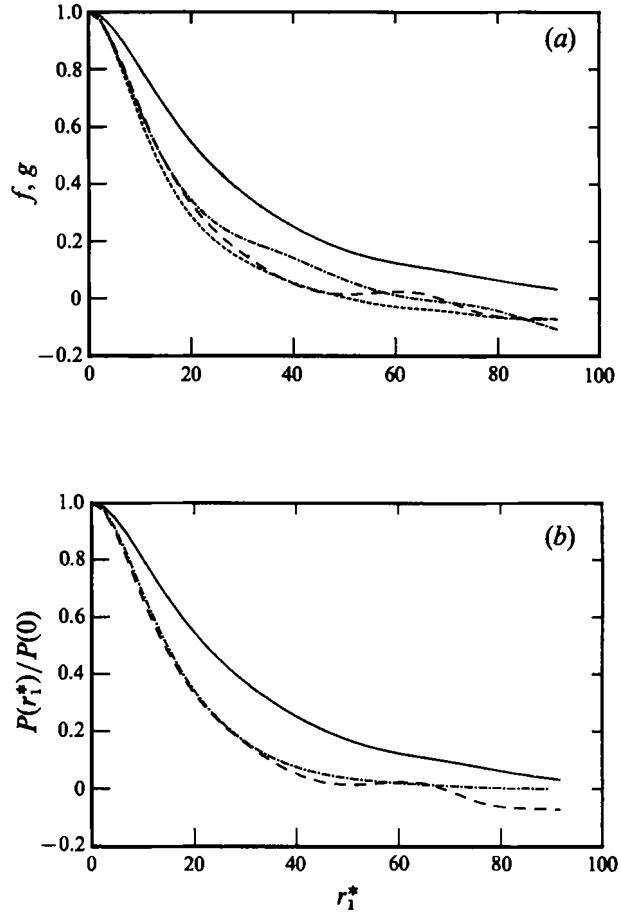

FIGURE 8. Velocity and pressure correlations at small longitudinal separations ($x_2/h = 1$). (*a*) Longitudinal and lateral velocity correlation coefficients ——, $f \equiv \overline{u_1(x_1)u_1(x_1+r_1)}/\overline{u_1^2}$, DNS. g: – – –, $\overline{u_2(x_1)u_2(x_1+r_1)}/\overline{u_2^2}$, DNS; — – —, $\overline{u_3(x_1)u_3(x_1+r_1)}/\overline{u_3^2}$, DNS; ——, calculated from (23). (*b*) Pressure correlation coefficients. (The longitudinal velocity correlation coefficient f is also shown (——).) $P(r_1)/P(0)$: – – –, DNS; ——, calculated from (20).

that shown in figure 4 at high wavenumbers. Comparison of figure 8 (*a* and *b*) indicates that the shape of $P(r_1)$ is much more similar to that of $g(r_1)$ than $f(r_1)$. This similarity has been noted by Hunt *et al.* (1987) who carried out a direct spectral simulation of nearly isotropic turbulence. These authors commented that for a distribution of Townsend-type large-scale eddies, the pressure variation across an eddy should be similar to that using u_2. The value of $P(0)$ calculated by Hunt *et al.* using (20) was about 7% lower than the pressure variance obtained in their simulation.

In Batchelor's (1951) calculation, fourth-order moments of velocity fluctuations were assumed to be related to second-order moments by

$$\overline{u_i u_j u_l' u_m'} = \overline{u_i u_j}\,\overline{u_l' u_m'} + \overline{u_i u_l'}\,\overline{u_j u_m'} + \overline{u_i u_m'}\,\overline{u_j u_l'},$$

where the unprimed and primed quantities refer to points x and x' ($\equiv x+r$) respectively. When all the indices are equal to 1, the above relation reduces to

$$\overline{u_1^2 u_1^2(r)} = \overline{u_1^2}^2 + 2\overline{u_1 u_1(r)}^2. \tag{22}$$

The validity of (22) was checked for the present data at the centreline with $r \equiv r_1$ and

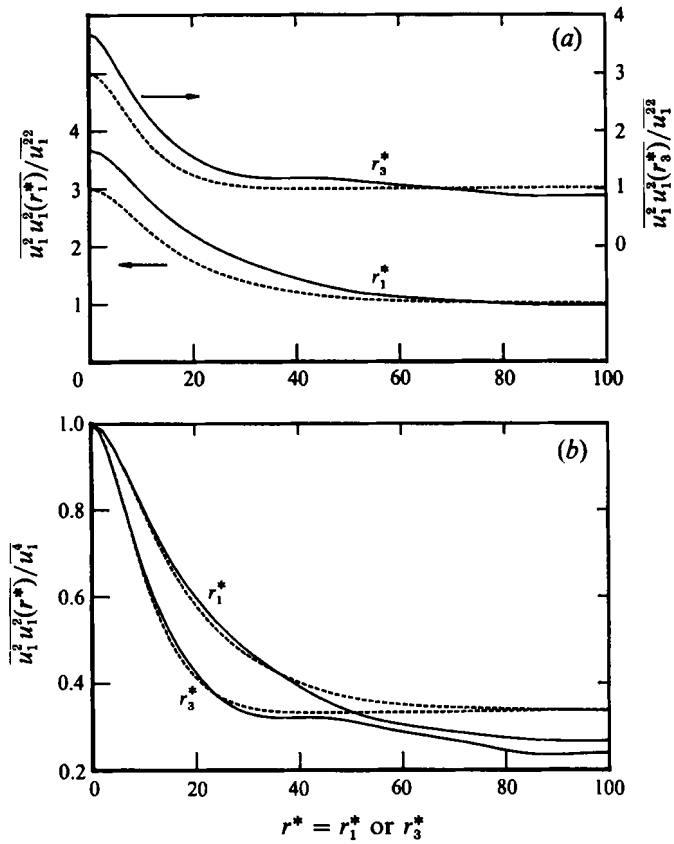

FIGURE 9. Comparison between fourth-order and second-order correlations of u_1 ($x_2/h = 1$). (*a*) Left- (——) and right-hand sides (– – –) of (22), normalized by $\overline{u_1^2}^2$. (*b*) Left- (——) and right-hand sides (– – –) of (22), normalized by their respective values at $r_1 = 0$ or $r_3 = 0$.

$r \equiv r_3$. The resulting distributions are shown in figure 9(*a*), where the normalization is by $\overline{u_1^2}^2$, and in figure 9(*b*), where each side of (22) is normalized by its own value at $r = 0$. At sufficiently large values of r, $\overline{u_1 u_1(r)}$ should become negligible and $\overline{u_1^2 u_1^2(r)}/\overline{u_1^2}^2$ should approach 1. This is indeed what figure 9(*a*) indicates, consistent with Batchelor's expectation that (22) is more likely to apply in the energy-containing range of r than at small separations. As $r \to 0$, $\overline{u_1^2 u_1^2(r)}/\overline{u_1^2}^2$ should approach 3 for a Gaussian distribution. Figure 9(*a*) shows that this is not the case, the flatness factor $\overline{u_1^4}/\overline{u_1^2}^2$ being equal to about 3.68 (it is reasonable to attribute this departure from Gaussianity to the small scales; one would also expect the departure to increase with Reynolds number). When the normalization of each side of (22) is by its own value at $r_1 = 0$ (or $r_3 = 0$), the two sides of the equation are practically identical for values of r_1^* (or r_3^*) extending up to about 40. This agreement reflects that between $P(r)/P(0)$ and Batchelor's calculation. This seems reasonable since only derivatives of the fourth-order velocity product enter the calculation.

7. Dependence on Reynolds number

The present data have been obtained at small values of the Reynolds number. Low Reynolds number effects are therefore expected to influence the statistics of the velocity and scalar fields everywhere in the flow. The effect of Reynolds number on the

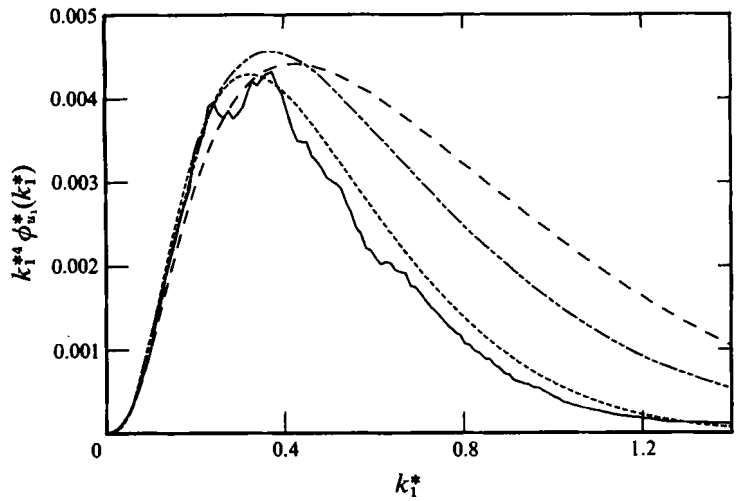

FIGURE 10. Dependence on Reynolds number of streamwise wavenumber spectrum of u_1, weighted by k_1^{*4} ($x_2/h = 1$). ——, present ($R_{\lambda_1} = 53$). The other three distributions ($R_{\lambda_1} = 98$ (– – – –), 443 (— — — —), 4950 (— — — —)) are those of Champagne (1978).

Reynolds stresses has been examined by Antonia *et al.* (1992), while the influence of h^+ on the statistics of vorticity and turbulent energy dissipation was detailed in Antonia *et al.* (1991). In the present context, it is appropriate to consider how the high-wavenumber part of the spectra varies with Reynolds number.

Champagne (1978) examined the Reynolds number dependence of spectra of $u_{1,1}$ (and also $u_{2,1}$) measured in different flows. He concluded that the Kolmogorov-normalized spectra are universal, only in the sense that they uniquely describe the high-wavenumber behaviour in different flows at the same value of R_{λ_1}. He also found that the high-wavenumber spectra evolved with R_{λ_1} in a manner consistent with the modified hypothesis of Kolmogorov. An appropriate way to examine this evolution is to plot $k_1^{*4}\phi_{u_1}^*$, which emphasizes the high-wavenumber part of the spectrum, as a function of k_1^*. The location of the present $k_1^{*4}\phi_{u_1}^*$ distribution in figure 10 appears to be consistent with the trend observed by Champagne† (his distributions at $R_{\lambda_1} = 98$, 443 and 4950 corresponding to a plane wake, circular jet and atmospheric boundary layer respectively). George (1989) has suggested that the high-wavenumber variation exhibited by Champagne's spectra need not be due solely to the increase in R_{λ_1} but may also reflect the difference in large-scale anisotropy for the different flows. Gagne & Castaing (1991) proposed a method for collapsing the spectra of Champagne and others using a presentation that is incompatible with Kolmogorov's (1941) similarity hypothesis. However, their proposal only extends down to $R_\lambda \approx 130$, and does not apply to the values of R_{λ_1} in the present simulations.

For isotropic turbulence, the equation for the mean-square fluctuating vorticity reduces to (e.g. Champagne 1978)

$$-\overline{u_{1,1}^3} = 2\nu\overline{u_{1,11}^2}$$

or

$$S_{u_{1,1}} = -116\int_0^\infty k_1^{*4}\phi_{u_1}^*\,\mathrm{d}k_1^*, \tag{23}$$

† These values are lower than those given in Champagne's paper by a factor of $\sqrt{2}$ because of a different definition of R_{λ_1} in the latter.

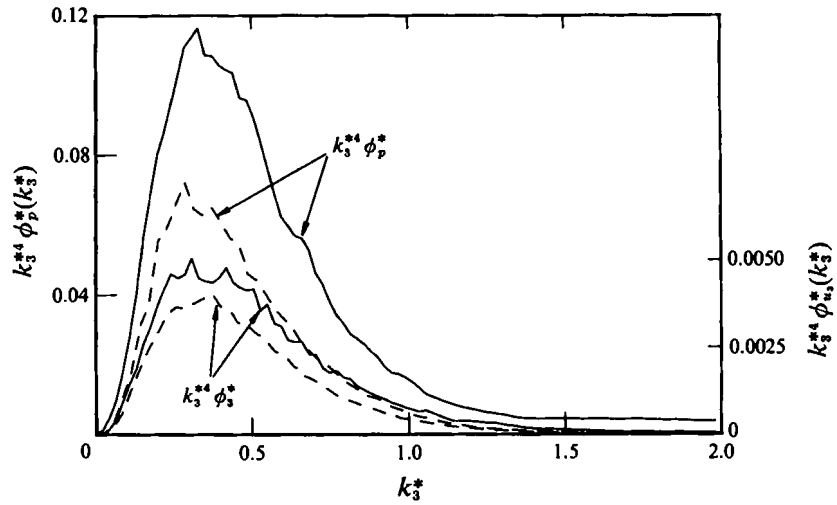

FIGURE 11. Reynolds number dependence of spanwise wavenumber spectra of u_1 and p, weighted by k_3^{*4} ($x_2/h = 1$). ——, $R_{\lambda_1} = 33$; ——, $R_{\lambda_1} = 53$.

where $S_{u_{1,1}} \equiv \overline{u_{1,1}^3}/\overline{u_{1,1}^2}^{\frac{3}{2}}$ is the skewness of $u_{1,1}$. Using (23), the area under the present distribution in figure 10 indicates a value of $S_{u_{1,1}}$ of -0.51 compared with an estimate of -0.49 for the left-hand side of (23). This agreement, notwithstanding the small value of R_{λ_1}, is due to the high-wavenumber weighting of the terms in the vorticity equation. It shows a correspondence between spatially local and spectral (small-scale) isotropy. Recently, Sanada (1992) showed, using direct numerical simulation of homogeneous stationary turbulence ($R_{\lambda_1} \approx 120$) that the dissipation range of the $E(k)$ spectrum was in close agreement with the exponential decaying form $k^{-\frac{1}{3}}\exp(-\sigma k^*)$, where σ is a constant. This form is also supported by the present data, despite the lack of an inertial subrange. Sanada's form of the spectrum is however Reynolds-number independent, a result which (see below) does not appear to be supported by the data of figure 10.

Spectra of velocity, vorticity and pressure fluctuations were also obtained using DNS data on the channel centreline with $h^+ = 180$ ($R_{\lambda_1} = 33$). (Details for this simulation can be found in Antonia *et al.* 1991, 1992.) The high-wavenumber behaviour of these spectra was also found to be consistent with small-scale isotropy. The maximum value of k_1^* attained at this boundary condition was only equal to 0.6 because the spacing Δx_1^+ between collocation points in the x_1 direction was equal to 11 (as compared with $\Delta x_1^+ \approx 7$ for $h^+ = 395$). Since the same value of Δx_3^+ was used at both Reynolds numbers, it seems more relevant to compare spanwise (instead of streamwise) wavenumber spectra at $R_{\lambda_1} = 33$ and $R_{\lambda_1} = 53$. The distributions (figure 11) of $k_3^{*4}\phi_{u_3}^*$ and $k_3^{*4}\phi_p^*$ show a significant increase in the Kolmogorov normalized spectrum, notwithstanding the relatively small increase in R_{λ_1}. Although the data have been obtained for the same location (i.e. $S = 0$) in the same flow, the above increase is likely to reflect the Reynolds number evolution of the whole spectrum – resulting from the low values of R_{λ_1} – and does not necessarily invalidate the suggestion by George (1989) that 'the Reynolds number variation observed by Champagne (1978) may be simply a measure of the fact that the flows themselves were different'.

It is of interest to compare the present pressure spectra at $R_{\lambda_1} = 53$ with the pressure spectra measured by Jones *et al.* (1979) in the mixing layer of a circular jet. The latter measurements were presented over the range $2 \leqslant x_1/D \leqslant 6$ (D is the jet diameter and

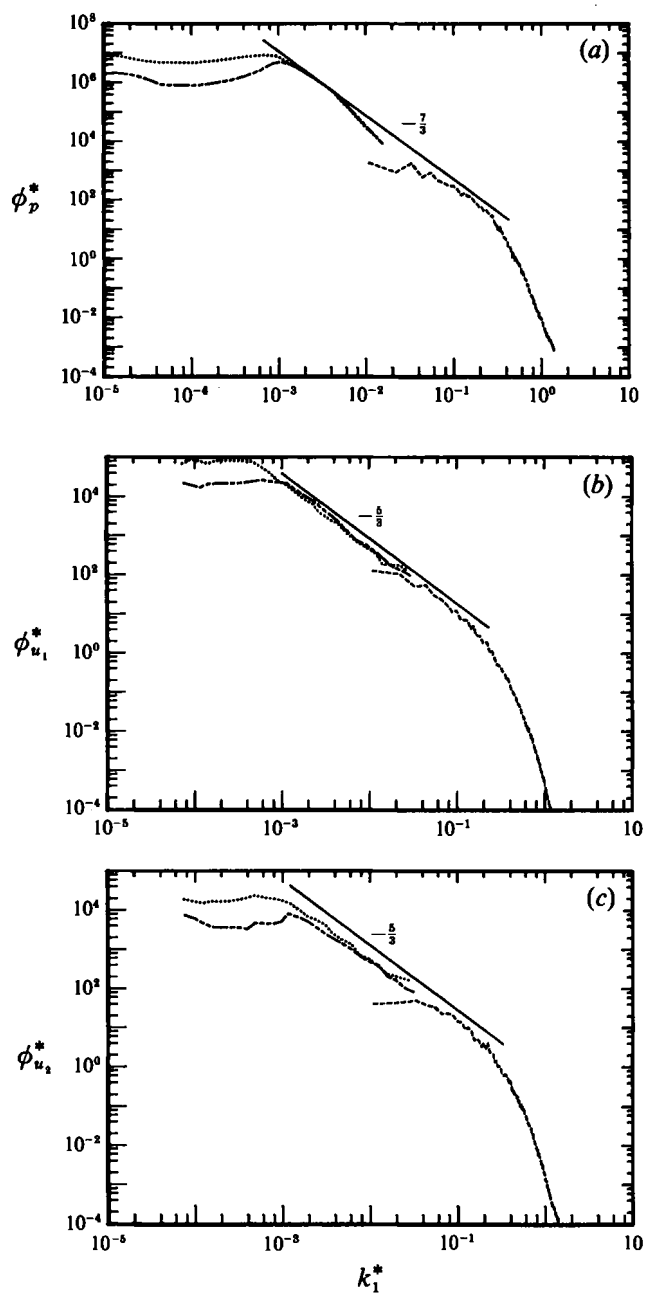

FIGURE 12. Comparison between the centreline pressure and velocity spectra with those of Jones *et al.* (1979). (*a*) ϕ_p^*; (*b*) $\phi_{u_1}^*$; (*c*) $\phi_{u_2}^*$. Jones *et al.* ———, $R_{\lambda_1} = 466$; - - - -, $R_{\lambda_1} = 841$; – – –, present ($R_{\lambda_1} = 53$); ——, $k_1^{*-\frac{7}{3}}$ for (*a*) or $k_1^{*-\frac{5}{3}}$ for (*b*) and (*c*).

x_1 is measured from the jet exit plane). The values of R_{λ_1}, inferred from the data of Jones *et al.* increase from about 466 at $x_1/D = 2$ to 841 at $x_1/D = 6$. The measured pressure spectra shown in figure 12(*a*) extend to values of k_1^* near the start of the $k_1^{*-\frac{7}{3}}$ inertial subrange. The location of the present spectrum suggests that the inertial subrange for the Jones *et al.* experiments should extend up to $k_1^* \approx 0.1$. For $k_1^* > 0.1$, the present pressure spectrum provides a plausible extension of the Jones *et al.*

spectrum to high wavenumbers; the extension seems justified given that the roll-off in the measured pressure spectra may be attributed to probe roll-off due to spatial averaging (George *et al.* 1984). The present distributions of $\phi^*_{u_1}$ and $\phi^*_{u_2}$ (figure 12*b*, *c*) are also plausible extensions (to the dissipation range) of the $k_1^{*-\frac{5}{3}}$ inertial subrange exhibited by the Jones *et al.* (1979) velocity spectra.

8. Conclusions and discussion

Low Reynolds number DNS data on the centreline of a fully developed turbulent channel flow are generally in good agreement with spectral local isotropy. The behaviour of high-wavenumber spectra of velocity, vorticity and pressure fluctuations is adequately described by the appropriate isotropic relations.

The high-wavenumber pressure spectrum compares favourably with Batchelor's (1951, 1953) analysis which provides an expression for the three-dimensional pressure spectrum in terms of the three-dimensional energy spectrum. Equivalently, the shape of the two-point pressure correlation is in good agreement with Batchelor's calculation for small longitudinal separations. For such separations, the shape of the two-point quadruple velocity correlation is also in good agreement with that implied by the joint normality assumption in Batchelor's theory.

The high-wavenumber isotropy exhibited by the results of §§4 and 5 supports the idea that small scales are close to being isotropic, in spite of the absence of an inertial subrange. This absence implies that a large separation between the energy-containing lengthscales and the dissipative lengthscales is apparently not needed before the latter become isotropic. This issue as well as the need to better define conditions under which small scales may tend to a universal form are clearly of interest (e.g. Phillips 1991; Hunt & Vasilicos 1991; Sreenivasan 1991). For example, in the context of decaying oceanic turbulence, Phillips (1991) observed that the Kolmogorov scaling of the high-wavenumber part of the spectrum need not imply a Kolmogorov-type energy cascade. The apparent insensitivity of the small scales to the large-scale anisotropy, as reflected by the present data, appears to be somewhat inconsistent with that of Domaradzky & Rogallo (1991) and Brasseur (1991), which point to strong non-local interactions between small and large wavenumbers. Such interactions would suggest that the small scales feel the straining motions by large scales and could therefore be anisotropic. It is possible, however, that although individual triad interactions are highly non-local (in wavenumber space), they may average out so that the net effect on the anisotropy of the small-scale motion is negligible (R. S. Rogallo, private communication).

The analysis by Durbin & Speziale (1991) has shown that the dissipation rate tensor cannot be isotropic if the mean strain rate is not zero. At $x_2/h = 0.4$, the mean strain rate is not negligible and the computed dissipation rate tensor is anisotropic. Yet figure 6(*c*) suggests that the small-scale pressure fluctuations satisfy isotropy as well as on the centreline (figure 5*c*). The strain at $x_2/h = 0.4$ produces an anisotropy which seems to shift the high-wavenumber velocity spectrum, but, in log–log coordinates, does not greatly alter its shape from that predicted by small-scale isotropy. As noted in §5, a better measure of the departure from isotropy is required before the effect of parameters such as $S\overline{q^2}/\bar{\epsilon}$ on small scales of the turbulence can be assessed unambiguously. Such an investigation is currently underway by the present authors.

As is well known, the assumption of local isotropy allows a considerable simplification when estimates of quantities such as $\bar{\epsilon}$ are required through measurement. The present centreline spectra show that the departure from isotropy is negligible at high wavenumbers and relatively small at low wavenumbers. Accordingly, the

assumption of isotropy yields a sufficiently accurate estimate of $\bar{\epsilon}$ at this location (see Antonia *et al.* 1991). As the distance from the centreline (and therefore the magnitude of S) increases, the assumption becomes less adequate. It was shown in Antonia *et al.* that the assumption of local axisymmetry is more accurate (though less easy to implement) than local isotropy. Near the wall, both assumptions are tenuous; in this region, the experimenter may derive some comfort from the fact that the major contributions to $\bar{\epsilon}$ reside in only a few terms (see figure 4 of Antonia *et al.* 1991) and that the most important of these, viz. $\overline{u_{1,2}^2}$, appears to be amenable to measurement (Zhu, Antonia & Kim 1993).

We are very grateful to Dr P. A. Durbin, Dr R. S. Rogallo and Professor A. M. Yaglom for their comments on the manuscript. R. A. A. acknowledges the support by the Australian Research Council.

REFERENCES

ANTONIA, R. A., ANSELMET, F. & CHAMBERS, A. J. 1986 Assessment of local isotropy using measurements in a turbulent plane jet. *J. Fluid Mech.* **163**, 365–391.

ANTONIA, R. A., BROWNE, L. W. B. & SHAH, D. A. 1988 Characteristics of vorticity fluctuations in a turbulent wake. *J. Fluid Mech.* **189**, 349–365.

ANTONIA, R. A., KIM, J. & BROWNE, L. W. B. 1991 Some characteristics of small-scale turbulence in a turbulent duct flow. *J. Fluid Mech.* **233**, 369–388.

ANTONIA, R. A., SHAH, D. A. & BROWNE, L. W. B. 1987 Spectra of velocity derivatives in a turbulent wake. *Phys. Fluids* **30**, 3455–3462.

ANTONIA, R. A., SHAH, D. A. & BROWNE, L. W. B. 1988 Dissipation and vorticity spectra in a turbulent wake. *Phys. Fluids* **31**, 1805–1807.

ANTONIA, R. A., TEITEL, M., KIM, J. & BROWNE, L. W. B. 1992 Low Reynolds number effects in a fully developed turbulent channel flow. *J. Fluid Mech.* **236**, 579–605.

BATCHELOR, G. K. 1951 Pressure fluctuations in isotropic turbulence. *Proc. Camb. Phil. Soc.* **47**, 359–374.

BATCHELOR, G. K. 1953 *The Theory of Homogeneous Turbulence*. Cambridge University Press.

BRASSEUR, J. G. 1991 Comments on the Kolmogorov hypothesis of isotropy in the small scales. *AIAA*-91-0230, *29th Aerospace Sciences Meeting, January 7-10, 1991, Reno, Nevada.*

CHAMPAGNE, F. H. 1978 The fine-scale structure of the turbulent velocity field. *J. Fluid Mech.* **86**, 67–108.

CHAMPAGNE, F. H., HARRIS, V. G. & CORRSIN, S. 1970 Experiments on nearly homogeneous turbulent shear flow. *J. Fluid Mech.* **41**, 81–139.

COMTE-BELLOT, G. 1963 Turbulent flow between two parallel walls. Université de Grenoble (translated by P. Bradshaw, *Rep. ARC* 31609 FM4/02, 1969).

DOMARADZKY, J. A. & ROGALLO, R. S. 1991 Local energy transfer and nonlocal interactions in homogeneous, isotropic turbulence. *Phys. Fluids* A **2**, 413–426.

DURBIN, P. A. & SPEZIALE, C. G. 1991 Local anisotropy in strained turbulence at high Reynolds numbers. *Trans. ASME* I: *J. Fluids Engng.* **113**, 707–709.

FUNG, J. C. H., HUNT, J. C. R., MALIK, N. A. & PERKINS, R. A. 1992 Kinematic simulation of homogeneous turbulence by unsteady random Fourier modes. *J. Fluid Mech.* **236**, 281–318.

GAGNE, Y. & CASTAING, B. 1991 Une représentation universelle sans invariance globale d'échelle des spectres d'énergie en turbulence développée. *C. R. Acad. Sci. Paris* **312** (II), 441–445.

GEORGE, W. K. 1989 The self-preservation of turbulent flows and its relation to initial conditions and coherent structures. In *New Horizons in Turbulence* (ed. W. K. George & R. Arndt), pp. 39–674. Hemisphere.

GEORGE, W. K., BEUTCHER, P. D. & ARNDT, R. E. A. 1984 Pressure spectra in turbulent free shear flows. *J. Fluid Mech.* **148**, 155–191.

HEISENBERG, W. 1948 Zur Statischen Theorie der Turbulenz. *Z. Phys.* **124**, 628–657.

HINZE, J. O. 1975 *Turbulence*. McGraw-Hill.

HUNT, J. C. R., BUELL, J. C. & WRAY, A. A. 1987 Big whorls carry little whorls. In *Proc. First Summer Program of the Center for Turbulence Research, Rep.* CTR-S87, pp. 79–94 NASA Ames/Stanford University.

HUNT, J. C. R. & VASILICOS, J. C. 1991 Kolmogorov's contributions to the physical and geometrical understanding of small-scale turbulence and recent developments. *Proc. R. Soc. Lond.* A **434**, 183–210.

JONES, B. G., ADRIAN, R. J., NITHIANANDAN, C. K. & PLANCHON, H. P. 1979 Spectra of turbulent static pressure fluctuations in jet mixing layers. *AIAA J.* **17**, 449–457.

KIM, J. 1989 On the structure of pressure fluctuations in simulated turbulent channel flow. *J. Fluid Mech.* **205**, 421–451.

KIM, J., MOIN, P. & MOSER, R. 1987 Turbulence statistics in fully developed channel flow at low Reynolds number. *J. Fluid Mech.* **177**, 133–166.

KLEBANOFF, P. S. 1955 Characteristics of turbulence in a boundary layer with zero pressure gradient. *NACA Rep.* 1247.

KOLMOGOROV, A. N. 1941 The local structure of turbulence in an incompressible fluid with very large Reynolds numbers. *Dokl. Akad. Nauk. SSSR* **30**, 301–305.

LAUFER, J. 1953 The structure of turbulence in fully developed pipe flow. *NACA Rep.* 1174.

MESTAYER, P. 1982 Local isotropy and anisotropy in a high-Reynolds-number turbulent boundary layer. *J. Fluid Mech.* **125**, 475–503.

MESTAYER, P. & CHAMBAUD, P. 1979 Some limitation to measurements of turbulence micro-structure with hot and cold-wires. *Boundary-Layer Met.* **16**, 311–329.

MONIN, A. S. & YAGLOM, A. M. 1975 Statistical fluid mechanics. In *Mechanics of Turbulence* (ed. J. L. Lumley), vol. 2. MIT Press.

OBOUKHOV, A. M. 1949 Pressure fluctuations in a turbulent flow. *Dokl. Akad. Nauk SSSR* **66**, 17–20.

OBOUKHOV, A. M. & YAGLOM, A. M. 1951 Microstructure of a turbulent flow. *Prikl. Math. Mekh.* **15**, 3–26 (translated as *NACA Rep. TM* 1350, June 1953).

PANCHEV, S. 1971 *Random Functions and Turbulence*. Pergamon.

PHILLIPS, O. M. 1991 The Kolmogorov spectrum and its oceanic cousins: a review. *Proc. R. Soc. Lond.* A **434**, 125–138.

SANADA, T. 1992 Comment on the dissipation-range spectrum in turbulent flows. *Phys. Fluids* A **4**, 1086–1087.

SPALART, P. R. 1988 Direct simulation of a turbulent boundary layer up to $R_\theta = 1410$. *J. Fluid Mech.* **187**, 61–98.

SREENIVASAN, K. R. 1991 On local isotropy of passive scalars in turbulent shear flows. *Proc. R. Soc. Lond.* A **434**, 165–182.

UBEROI, M. S. 1953 Quadruple velocity correlations and pressure fluctuations in isotropic turbulence. *J. Aero. Sci.* **20**, 197–204.

VAN ATTA, C. W. 1977 Second-order spectral local isotropy in turbulent scalar fields. *J. Fluid Mech.* **80**, 609–615.

VAN ATTA, C. W. 1991 Local isotropy of the smallest scales of turbulent scalar and velocity fields. *Proc. R. Soc. Lond.* A **434**, 139–147.

ZHU, Y., ANTONIA, R. A. & KIM, J. 1993 Velocity and temperature derivative measurements in the near-wall region of a turbulent duct flow. To be presented at *Int. Conf. on Near-Wall Turbulent Flows, Tempe, Arizona.*